ISIJ International, Vol. 54 (2014), No. 7, pp. 1530–1538

Metal-slag Separation Behaviors of Pellets Consisted of Iron, Graphite and CaO–Al_2O_3 Based Slag Powders

Ji-Ook PARK,[1)]* In-Hyeon JEONG,[1)] Sung-Mo JUNG[1)] and Yasushi SASAKI[2)]

1) Graduate Institute of Ferrous Technology (GIFT), Pohang University of Science and Technology (POSTECH), Pohang, 790-784 South Korea. 2) School of Materials Science and Engineering, UNSW Australia, Sydney, 2052 Australia.

(*Received on December 16, 2013; accepted on March 10, 2014*)

In-situ observations of metal-slag separation behaviors between CaO–Al_2O_3 based slag, iron and graphite powder mixed pellets by a confocal laser-scanning microscope (CLSM) have been carried out to find the effective way to use high Al_2O_3 iron ore in CCA reduction processes. Since a particular type of high Al_2O_3 iron ore such as laterite contains small amount of NiO and Cr_2O_3, the effect of NiO and Cr_2O_3 on the metal-slag separation behaviors were also studied. The observed metal-slag separation behaviors were analyzed based on the equilibrium phase fractions calculated by FactSage and carbon diffusion simulation in an iron sphere particle with *a spot carbon source condition*. Based on these *in-situ* observations and carbon diffusion results, starting temperature of metal-slag separation was found to correspond to the eutectic temperature of CaO–Al_2O_3 based slag. The iron carburization was initiated by slag melting and most of iron particles were melted within about 20 s after slag melting. The rapid carburization after slag melting was introduced by the good wettability between solid iron and molten slag. NiO and Cr_2O_3 additions did not change the fundamental behaviors of metal-slag separation at least up to about 3 mass%. Based on these results, it was confirmed that high Al_2O_3 content iron ore can be used in CCA reduction process by using CaO–Al_2O_3 based slag.

KEY WORDS: metal-slag separation; high Al_2O_3 iron ore; iron carburization; spot source diffusion; CaO–Al_2O_3 based slag.

1. Introduction

Due to the depletion of high-grade iron ore resources in the world, high Al_2O_3 iron ores have been forced to use. The change of iron-ore compositions is resulting in some problems for blast furnace (BF) operation. In the sintering process, the low fluidity due to the increase of Al_2O_3 content produces uneven sinter ore properties in the sintering bed, and the increase of Al_2O_3 tends to produce coarse calcium ferrite phase which brings bonding strength degradation and the low reduction degradation index.[1,2)] In BF operation, high Al_2O_3 content in the slag causes poor slag discharging due to its high viscosity and increase of slag volume as well.

In direct reduced iron (DRI) processes, however, the slag composition is not so demanding compared with that of BF process. Consequently, DRI process will be one of the possible choices to effectively use high Al_2O_3-containing iron ore. In coal-based DRI processes, fine iron ore and coal are agglomerated in the form of carbon composite agglomerate (CCA), and CCA is reduced to iron by using a rotary hearth furnace or rotary kiln.[3–5)] In CCA smelting reduction processes, good metal-slag separation is practically important to avoid extra cost and time for final iron nuggets.

In the current coal-based DRI processes with low Al_2O_3 iron ores, the finally formed slag compositions are in the region of 'a', 'b' and 'c' shown in **Fig. 1** due to their low melting temperature and the ease of slag composition control. Consequently, the coal-based CCA reduction behaviors with the slag composition 'a', 'b' and 'c' have been well studied.[6–10)] However, these slag compositions are not suitable

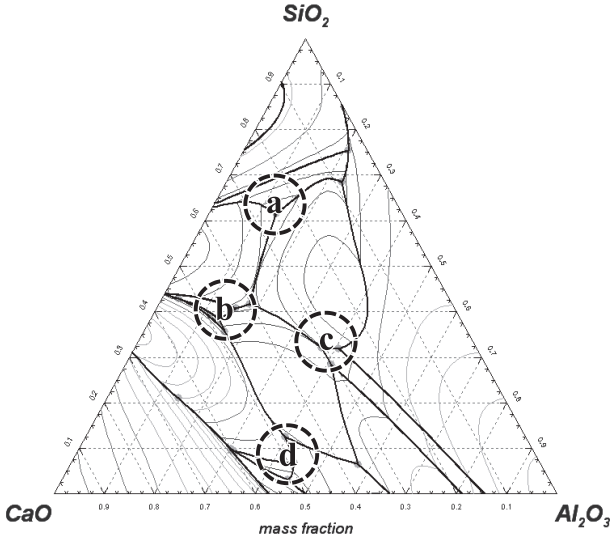

Fig. 1. Low melting temperature slag regions in CaO–Al_2O_3–SiO_2 ternary phase diagram.

* Corresponding author: E-mail: damanegy@postech.ac.kr
DOI: http://dx.doi.org/10.2355/isijinternational.54.1530

for high Al_2O_3 iron ore due to the increase of slag volume. Thus, to effectively and extensively use high Al_2O_3-containing iron ores with CCA reduction process, alternative slag design must be developed.

Among high Al_2O_3 iron ores, some of them contain low SiO_2 content. To use this type of iron ores, $CaO–Al_2O_3$ based slag in the region 'd' (Fig. 1) is attractive because of small amount of requiring additives to design the suitable slag composition and its low slag melting temperature. It has been also found that the viscosity of the slag in the region 'd' is similar to those of slags in the regions of 'a', 'b' and 'c'.[11)]

The coal-based direct reduction process consists of several steps of (1) iron ore reduction, (2) carburization & melting of reduced iron, (3) slag melting, (4) metal-slag separation and molten iron coalescence. These steps with the slag region 'a', 'b' and 'c' have been already studied.[6–8,12)] Ohno *et al.*[6)] investigated the effect of metal-slag separation based on slag melting temperatures and viscosities with slag region 'b' and 'c'. Nogueira *et al.*[7)] also observed clear metal-slag separation behavior with slag 'a'. Kim *et al.*[8,12)] studied the role of liquid phase on the metal-slag wetting/separation behavior in the slag composition 'a' based on *in-situ* confocal laser-scanning microscope (CLSM) observation. But none of them focused on the metal-slag separation behavior of the slag region 'd' which can be practically important to use high Al_2O_3 ore for CCA reduction process.

In the present study, as a first step study to effectively use high Al_2O_3 iron ore in CCA reduction process, the metal-slag separation behaviors of the pellets consisted of the mixtures of iron, graphite and $CaO–Al_2O_3$ based slag particles have been investigated. Since a particular type of high Al_2O_3 with low SiO_2 iron ore such as laterite sometimes contains small amount of NiO and Cr_2O_3, the effect of NiO and Cr_2O_3 on the metal-slag separation behaviors were also studied. Based on these results, the role of molten slag and the effect of carburization rate on metal-slag separation were also discussed.

2. Experimental

Ohno *et al.* carried out *in-situ* CLSM observation to clarify the effect of slag melting on metal-slag separation.[6)] Experimental details in this study were almost the same with their method except using $CaO–Al_2O_3$ based slag.

2.1. Preparation of Samples

Synthetic slags were prepared by melting the compressed mixture of chemical grade CaO, Al_2O_3 and SiO_2 at 1 773 K in Ar atmosphere. After holding for 24 hours at 1 773 K, the molten slag was quenched by pouring on a water cooled Cu plate to make glassy materials. After crushing and sieving the glassy slag, X-ray fluorescence analysis was used to confirm the slag composition. Compositions of the synthetic slag were shown in **Table 1**. Since the melting point of slag sample D is higher than 1 773 K, some amount of unmelted solid slag phase could exist in the quenched sample. To minimize the effect of the solid phase existence, the quenched samples were fully ground with the size of around 45 μm–100 μm and well mixed.

To find the effect of NiO and Cr_2O_3 on metal-slag separation behaviors, 0.99, 1.96 and 3.85 mass% of Cr_2O_3 and 0.99, 1.96 and 3.85 mass% of NiO were added in slag B to slag G, respectively. Small amount of Cr_2O_3 greatly increases melting temperature of the $CaO–Al_2O_3$ based slag, while NiO does not as shown in Table 1. Typical $CaO–Al_2O_3–SiO_2$ based slag H with low melting point was also prepared for comparison with $CaO–Al_2O_3$ based slag. "Melting temperature" of slag in this study is defined as temperature where all the solid phase disappears and was estimated from FactSage equilibrium calculation.

Table 1. Experimental slag compositions for *in-situ* observation.

Sample	Content (mass%)						Melting T (K)
	CaO	SiO_2	Al_2O_3	Cr_2O_3	NiO	CaO/SiO_2	
Slag A	52.00	6.60	41.40	0	0	7.9	1 690.77
Slag B	51.49	6.53	40.99	0.99	0	7.9	1 418.14
Slag C	50.98	6.47	40.59	1.96	0	7.9	1 737.97
Slag D	50.00	6.35	39.80	3.85	0	7.9	1 847.56
Slag E	51.49	6.53	40.99	0	0.99	7.9	1 690.79
Slag F	50.98	6.47	40.59	0	1.96	7.9	1 681.51
Slag G	50.00	6.35	39.80	0	3.85	7.9	1 665.04
Slag H	40.4	39.7	19.9	0	0	1.0	1 603.00

Table 2. Material mixing ratios between electrolytic iron, graphite and synthetic slag.

Electrolytic Iron (Mass%)	Graphite Powder (Mass%)	Synthetic Slag (Mass%)	Carbon Mixing ratio to Fe (Mass% base)	Slag Mixing ratio to Fe (Mass% base)
61.65	0.62	37.74	0.01	0.612
60.89	1.83	37.28	0.03	0.612
60.16	3.01	36.83	0.05	0.612
58.40	5.84	35.76	0.10	0.612

Prepared slag, electrolytic iron and graphite powders were mixed by a particular mixing ratio as shown in **Table 2**. Slag mixing ratio to Fe was fixed to 0.612 based on mass% ratio between total iron and gangue material in a particular type low SiO_2 containing limonitic Laterite ore.[13)] Graphite mixing ratio to Fe was changed to 0.01, 0.03, 0.05 and 0.10 based on mass% ratio. The sizes of iron source and graphite powders were –50 μm and that of synthetic slag powder was sieved to 45–100 μm. After homogeneously mixing synthetic slag, iron and graphite powders, this mixture was pressed with 5 MPa for 2 minutes by CIP method to make a pellet (Dia. 5 mm × height 2.5 mm).

2.2. Experimental Procedure

A CLSM was used for in-situ observation of CCA pellet melting behaviors with heating. A pressed pellet (about 50 mg) was put in the Al_2O_3 crucible (OD: 9 mm, ID: 8 mm) and placed to heating stage. Inner chamber was sealed and purged with high purity Ar before experiments and flow rate of 200 mL/min was kept during observation. The pellet was rapidly heated to 1 323 K with heating rate of 300 K/min and then maintained for 30 seconds at that temperature. After stabilization, the sample was heated to 1 773 K with 75 K/min heating rate. Although slight higher metal-slag

separation temperature was observed at 100 K/min heating rate than 75 K/min in the present study, the difference was less than 5 degree which can be neglected. Ohno[6] also reported that different heating rate did not make any differences in metal-slag separation temperature in the range of 10 K/min–100 K/min.

Whole processes with heating were observed and recorded to determine (1) iron melting start temperature, (2) metal-slag separation start temperature and (3) metal-slag separation finish temperature. The metal-slag separation start temperature was defined as being defocused temperature due to the start of liquid slag or iron droplets coalescence, and the metal-slag separation finish temperature was defined as a large spherical iron droplet shown-up temperature. After the confirmation of the metal-slag separation, the sample was rapidly cooled to room temperature to minimize carburization after the metal-slag separation. Thermodynamically Cr_2O_3 will not be reduced, but NiO can be reduced. However, the reduction of NiO in solid slag by solid carbon is not easy since it is difficult to contact each other. Therefore, we can assume that NiO would not be reduced before slag melting. In the preliminary experiments, it was found that about more than 5 min was required for the full NiO reduction. The difference between separation start time and finish time is about 24 sec. Therefore, it can be assumed that the effect of the NiO content decrease after slag melting due to NiO reduction on the metal-slag separation behavior will be small.

3. Results

3.1. *In-situ* Observation of Melting and Separation Behaviors

The observed melting and separation behaviors for slag A were shown in **Fig. 2**. They showed (a) Fe–C melt formation, (b) Slag melting initiation, (c) start of metal-slag separation (starting of coalescence of small metal droplets or slag droplets) and (d) accomplishment of metal-slag separation (a large liquid metal drop formation). These steps were observed in all experimental conditions except the pellet that had 1 mass% of graphite to Fe mixing ratio. In this case, full melting of Fe was not achieved. The observed metal-slag separation sequences of the pellets with $CaO–Al_2O_3$ based slag were almost the same with those of slags in the region 'a', 'b' and 'c' (shown in Fig. 1).

3.2. Effect of Carbon Mixing Ratio on Metal-slag Separation Behaviors

The iron melting start temperature, metal-slag separation start temperature and metal-slag separation finish temperature as a function of carbon mixing ratio to Fe were shown in **Fig. 3**. It was found that liquid Fe–C formation temperature was almost the same with Fe–C eutectic temperature of 1 420 K regardless of carbon mixing ratio, even with 1 mass% C mixing ratio. It was also found that metal-slag separation start temperature of about 1 603 K also did not depend on the carbon mixing ratio to Fe.

Since the melting point of Fe-1.0 mass% C alloy is

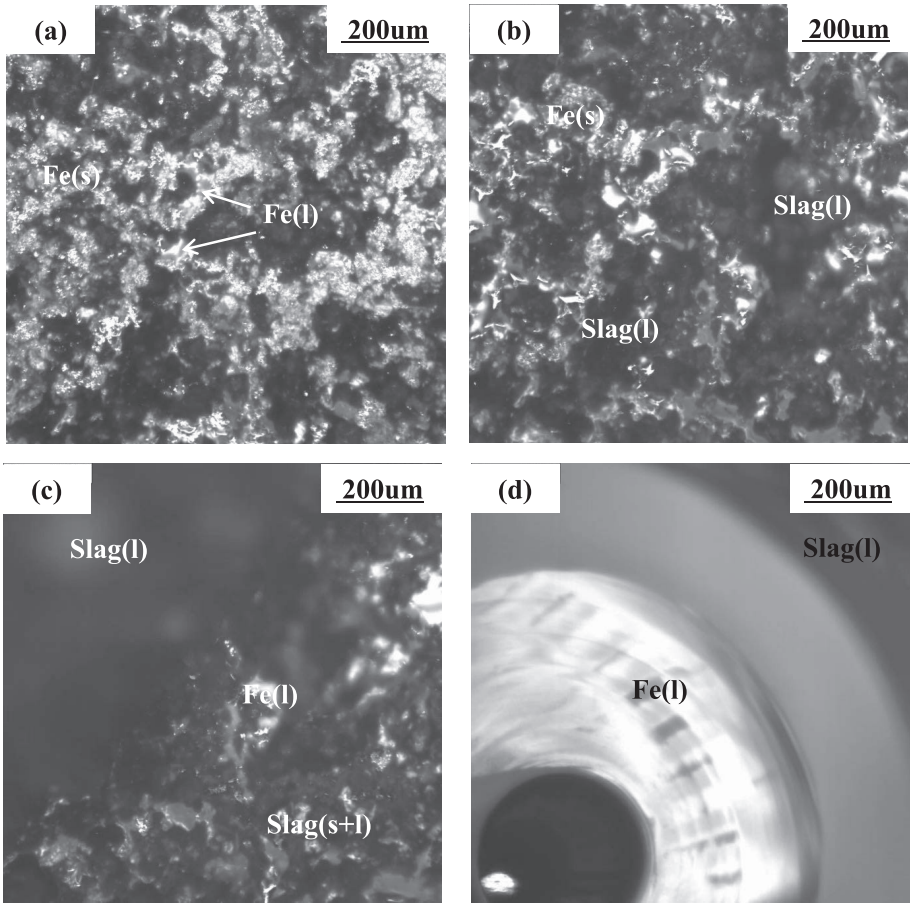

Fig. 2. Confocal *in-situ* observation images during heating. (a) Fe–C melt formation at eutectic temperature, (b) Slag melting initiation, (c) Metal-slag separation start and (d) Metal-slag separation finish.

around 1 623 K, the observed initiation of iron melting at 1 420 K for 1 mass% carbon mixing pellet means that some iron particles were carburized over 2.1 mass% while the remained part of iron particles was barely carburized. Possibly due to this reason, full metal-slag separation was not observed in the case of 1 mass% carbon mixing pellet, and the separation finish temperature with 3.0 mass% carbon mixing pellet was much higher than those with 5.0 and 10.0 mass% carbon mixing pellet. These results suggested that sufficient amount of carbon must be supplied to Fe particles to promote metal-slag separation. Therefore, in the present study, the metal-slag separation behaviors of pellets with 10.0 mass% C have been mainly studied. This carbon

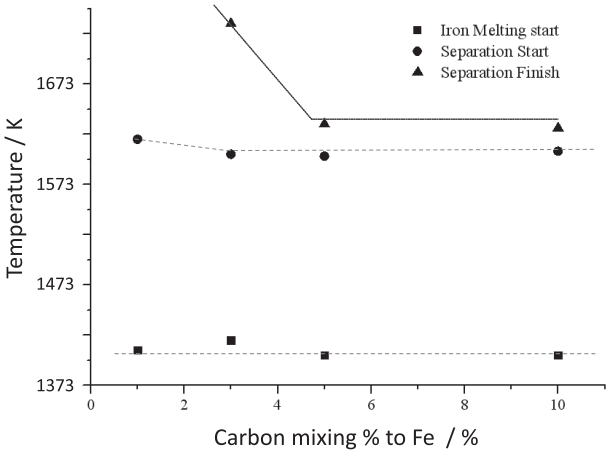

Fig. 3. The effect of carbon mixing ratio on iron melting start temperature, metal-slag separation start temperature and metal-slag separation finish temperature.

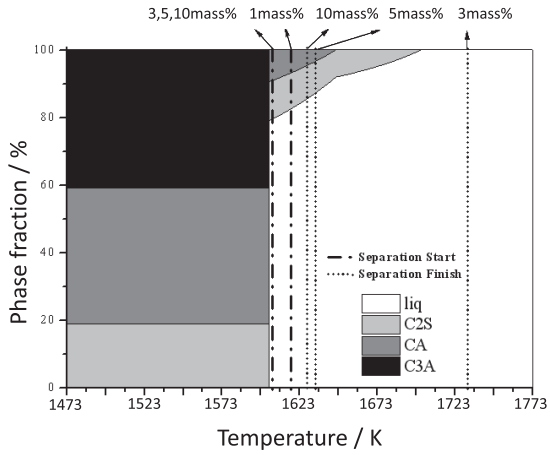

Fig. 4. Temperature dependence of equilibrium phase fraction of $CaO–Al_2O_3$ based slag. Liq: liquid phase, C2S: $CaO·2SiO_2$, CA: $CaO·Al_2O_3$, C3A: $3CaO·Al_2O_3$.

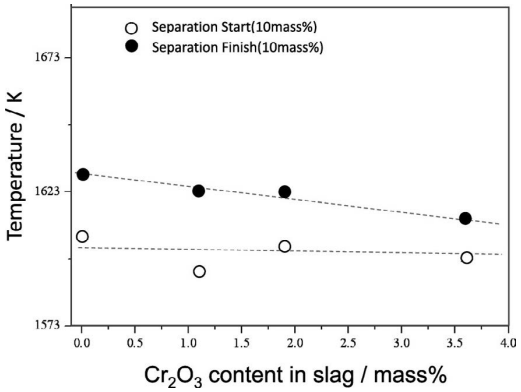

Fig. 5. The effect of Cr_2O_3 content on metal-slag separation start and finish temperature.

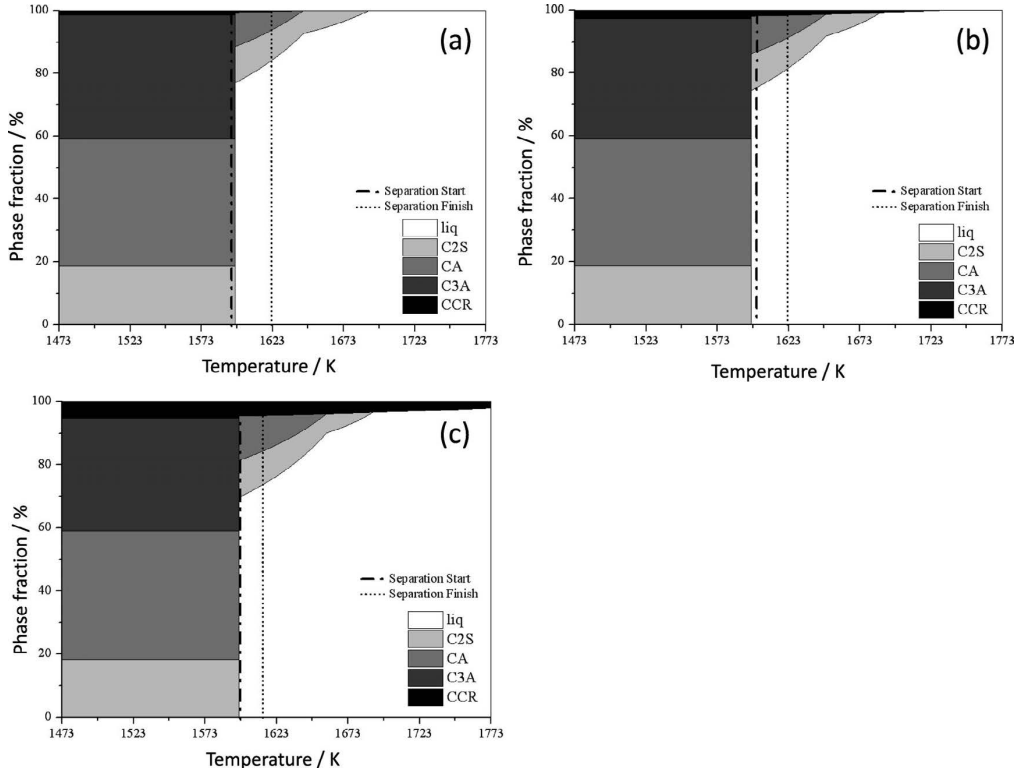

Fig. 6. Temperature dependence of equilibrium phase fraction in Cr_2O_3 containing $CaO–Al_2O_3$ based slags. (a) 0.99% Cr_2O_3, (b) 1.96% Cr_2O_3 and (c) 3.85% Cr_2O_3. Liq: liquid phase, C2S: $CaO·2SiO_2$, CA: $CaO·Al_2O_3$, C3A: $3CaO·Al_2O_3$, CCR: $CaCr_2O_4$.

content was enough to carburize iron at more than the concentration of eutectic point, but the observed large amount of the residual carbon after experiments indicates that carbon was not fully consumed.

As shown in Fig. 3, if carbon mixing ratio exceeds 5 mass% C, both of the separation start and finish temperatures were not affected by carbon mixing ration. This simply suggests that metal-slag separation behavior was mainly governed by slag melting and following iron melting but not the amount of carbon if carbon is sufficiently supplied. In other words, the excess carbon had negligibly small effect on the metal-slag separation behaviors.

To understand metal-slag separation behaviors, the equilibrium phase fraction of $CaO–Al_2O_3$ based slag (slag A) as a function of temperature was calculated by FactSage and shown in **Fig. 4** along with the metal-slag start and finish temperatures. A large amount of liquid phase (about 80%) suddenly formed at about 1 603 K by the eutectic reaction between $3CaO·Al_2O_3$ (C3A) and $CaO·Al_2O_3$ (CA) and $CaO·2SiO_2$ (C2S) phases, and this eutectic melting temperature is almost the same with the observed metal-slag separation start temperature shown in Fig. 3.

3.3. Effect of Cr_2O_3 and NiO Contents in Slags on Metal-slag Separation Behaviors

The metal-slag separation start and finish temperatures as a function of Cr_2O_3 content with carbon mixing ratio of 10 mass% were shown in **Fig. 5**. As shown in Fig. 5, the Cr_2O_3 addition did not show any distinct increase of separation start temperature in spite of melting point increase by Cr_2O_3 addition. The metal-slag separation finish temperatures slightly decreased with Cr_2O_3 content.

The calculated phase fraction changes of $CaO–Al_2O_3$ based slags with various Cr_2O_3 content as a function of temperature along with the metal-slag start and finish temperatures are shown in **Fig. 6**. A large amount of liquid phase was suddenly formed at the temperature of around 1 600 K due to the eutectic reaction. The metal-slag separation start temperatures of three different Cr_2O_3 containing slags were almost corresponded to eutectic melt formation temperature of each slag as like the case of $CaO–Al_2O_3$ based slag without Cr_2O_3.

The effect of NiO content on metal-slag separation start and finish temperature was shown in **Fig. 7**. The metal-slag separation start and finish temperature were dropped about 25 degree by a small addition of NiO and then gradually decreased with increase of NiO content. **Figure 8** shows the

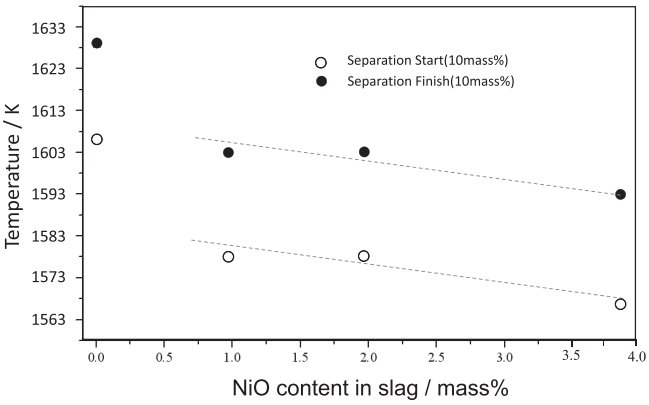

Fig. 7. The effect of NiO content on metal-slag separation start and finish temperature.

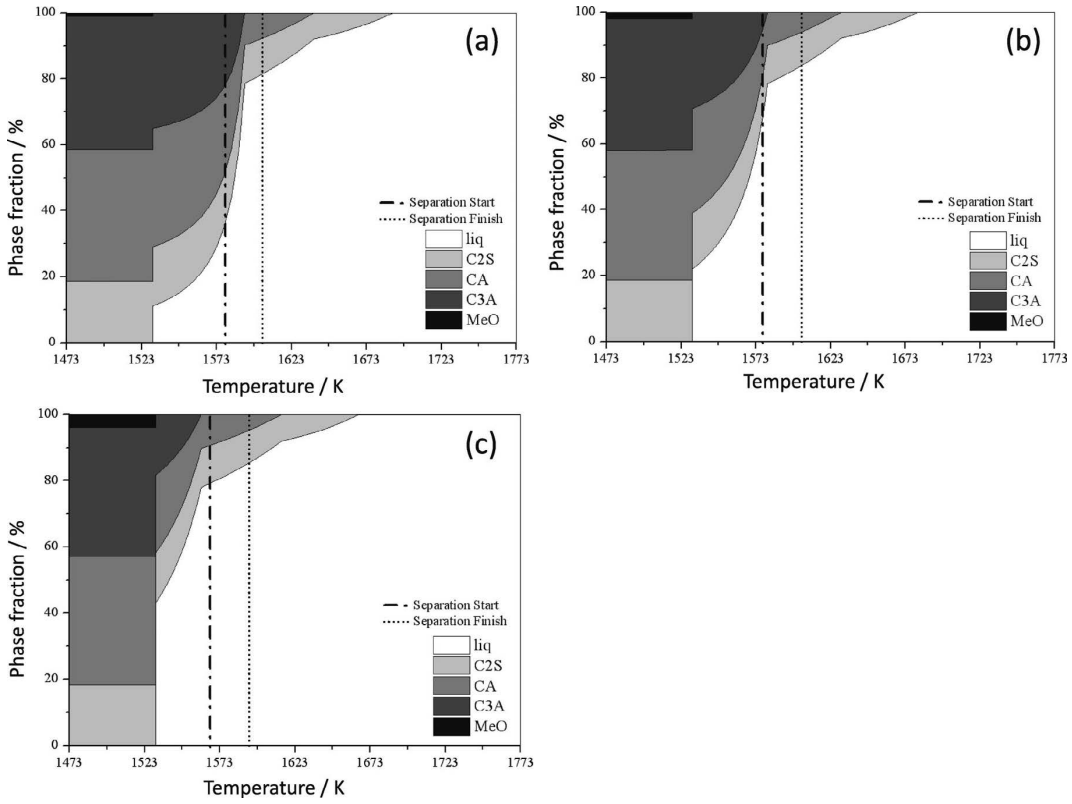

Fig. 8. Temperature dependence of equilibrium phase fraction in NiO containing $CaO–Al_2O_3$ based slags. (a) 0.99% NiO, (b) 1.96% NiO and (c) 3.85% NiO. Liq: liquid phase, C2S: $CaO·2SiO_2$, CA: $CaO·Al_2O_3$, C3A: $3CaO·Al_2O_3$, MeO: NiO.

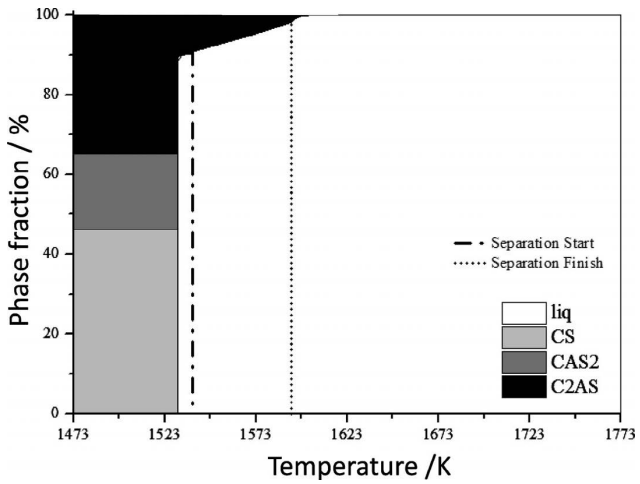

Fig. 9. Temperature dependence of equilibrium phase fraction in CaO–Al_2O_3–SiO_2 based slag. Liq: Liquid phase, CS: $CaO{\cdot}SiO_2$, CAS2: $CaO{\cdot}Al_2O_3{\cdot}2SiO_2$, C2AS: $2CaO{\cdot}Al_2O_3{\cdot}SiO_2$.

calculated phase fraction changes of CaO–Al_2O_3 based slag with various NiO contents as a function of temperature along with the metal-slag start and finish temperatures. As already mentioned, NiO was unlikely to be reduced before slag melting. Therefore, the phase fraction changes were calculated based on the initial NiO contents.

The eutectic liquid slag formation temperature was slightly lowered with increase of NiO contents. After the small amount of eutectic melt was formed, the amount of liquid phase was gradually increased with increase of temperature. The metal-slag separation in the slag with NiO additions started at the temperature of first inflection point after eutectic in liquid fraction curve except slag E. In case of slag E, liquid fraction changes from 30% to 80% in a very short temperature range so at the separation start temperature, more amount of slag can be existed than calculation. Interestingly, liquid slag fraction at the metal-slag separation start temperatures in base slag (as shown in Fig. 4) and Cr_2O_3 added slag (as shown in Fig. 6) were corresponded to liquid fraction at the first inflection point after eutectic of NiO contained slag.

3.4. Metal-slag Separation Behavior of Conventional CaO–Al_2O_3–SiO_2 Slag

The phase fraction changes of the conventional CaO–Al_2O_3–SiO_2 based slag (slag H) and temperature of separation start and finish with 10.0 mass% C are shown in **Fig. 9**. Slag H has relatively low melting temperature compared with CaO–Al_2O_3 based slag. The slag H almost started to melt at around 1 533 K, so the separation start temperature was also low compared with the high basicity slag. Nevertheless, temperature difference between separation start temperature and finish temperature in CaO–Al_2O_3–SiO_2 based slag is about 60 K which is more than two times higher than that of CaO–Al_2O_3 based slag. It simply implies metal-slag separation in slag H, iron and graphite mixture pellet is mainly governed by iron melting not by slag melting behavior.

4. Discussion

4.1. Particle Configuration

It is noted that metal-slag separation behaviors were controlled not only by thermodynamics but also kinetics. The slag melting is determined simply by temperature. The eutectic melt will be produced at the eutectic temperature and whole slag will be melted at the melting point.[14] However, iron melting will be controlled by iron carburization process. It means that iron melting will be strongly influenced by iron and graphite particles configurations such as the iron particle size, relative amounts of graphite with iron and contact condition between carbon and iron particles.

In the present study, the average particle size of iron, graphite and slag powders were about 50 μm, 50 μm and 70 μm, respectively. Since their particles diameters were relatively close, it is reasonable to assume that these particles were 3-dimensionally closely packed. By assuming the each particle shape is a sphere, the particle number fractions of iron, graphite and slag particles are about 0.52, 0.19 and 0.28, respectively, under the C/Fe ratio (mass% base) of 0.1. For the calculation, the density of Fe (7.6 g/cm^3), C (2.0 g/cm^3) and slag (3.0 g/cm^3) are used. In the closed packed structure the coordination number is 12. Thus, in the present experimental condition, one iron particle was supposed to contact with 6 iron particles, 3 slag particles and 2 graphite particles as a first approximation. Namely, the skeleton of the pellet was constructed by 3-dimensional closed packed iron particles and several iron particles were replaced by graphite and slag particles.

The particle configuration with Ohno *et al.*[6] was quite different. Their average particle size of iron, graphite and slag particles were about 150 μm, 25–32 μm and 25–32 μm, respectively. Under this condition, the large iron particles formed the skeleton of the pellet, and graphite and slag may occupy the space between the large iron particles. Namely, the contact condition between iron and graphite particles in the present study was quite different from that in Ohno *et al.*[6] The particle configurations of (a) the present study and (b) that with Ohno *et al.*[6] were schematically shown in **Fig. 10**. These different particle configurations possibly introduce different iron carburization behavior. Thus, simple comparisons among the experimental results about metal-slag separation behaviors without considering the particle configurations are misleading.

4.2. Carburization of Iron Particles

As already shown in Fig. 3, small amount of iron was melted at the eutectic temperature. However, most of iron remained as solid phase until slag melting, possibly due to the poor contacting between them. The carburization of iron particles during CCA reduction will be initiated from the *point* contact with carbon particles. Thus, the understanding of a spot source carbon diffusion process in iron particles is very important to investigate metal-slag separation process. Thus, the numerical simulation of the spot source carbon diffusion process was carried out in the present study.

The diffusion coefficient of carbon in austenite, D_C, depends on the carbon concentration and also liquid phase will be formed at the contacting spot with increase of carbon concentration.

To simplify the calculation, (1) the value of D_C was represented by the values at the average carbon content, (2) the liquid phase formation was neglected and (3) assuming the constant temperature of 1 573 K although actual diffusion

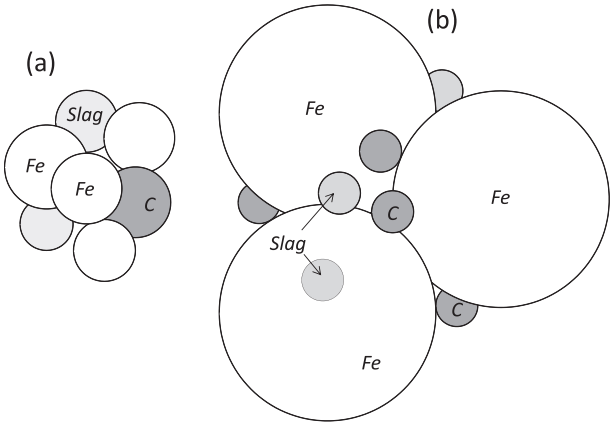

Fig. 10. Particle configurations of (a) the present study and (b) that with Ohno *et al*.[6]

process was non-isothermal as a first approximation. In this study, the following expression for D_C (m^2/s) by Ågren[15] was used,

$$D_c = 4.53\times10^{-7}\left(1+\frac{y_C(1-y_C)8\,339.9}{T}\right) \exp\left\{-\left(\frac{1}{T}-2.221\times10^{-4}\right)(17\,767-y_C 26\,436)\right\} \quad \ldots(1)$$

where $y_C = x_C/(1–x_C)$, x_C being the mole fraction of carbon and T is the absolute temperature. As shown in Figs. 6 and 8, the metal-slag separations started after at about 1 573 K. To understand this behavior, the C diffusion process in Fe particle at 1 573 K was evaluated as a first step. The C concentration at the spot is fixed to 1.3 mass%. The values of D_C at 1 573 K with average C concentration of 0.65 mass% was 4.90×10^{-10} m^2/s. The geometry of calculation is schematically shown in **Fig. 11**. The small circle was patched on the top of a Fe sphere particle (dia. 50 μm). The aim of the calculation is simply to examine the diffusion rate difference between under the spot source and the general surface boundary source conditions. Therefore, the simple sphere particle was used for the diffusion rate calculation in the present study although the actual shape of Fe particles is not sphere.

The circular area was used as the spot source of carbon. Under these conditions, the 3-dimensional carbon concentration distribution in the Fe sphere was solved by using commercial code COMSOL multiphysics. COMSOL numerically solved the following the diffusion equation of (2) as a function of time by using finite element method.

$$\frac{\partial C}{\partial t} = D_C \nabla^2 C \quad \ldots(2)$$

In the calculation, the mesh size near the spot source is set to 0.1 μm, and the mesh size far from the point source is 3 μm. The total number of the meshes was about 40 000.

The average carbon content (mass%) in the Fe particle as a function of time with various spot areas are shown in **Fig. 12**. The diffusion rates were increased with spot source areas as expected. In the case of surface source diffusion with the same conditions, the concentration reached to the surface concentration only after *0.1 second*. Namely, the diffusion rate with a spot source was quite slow compared with

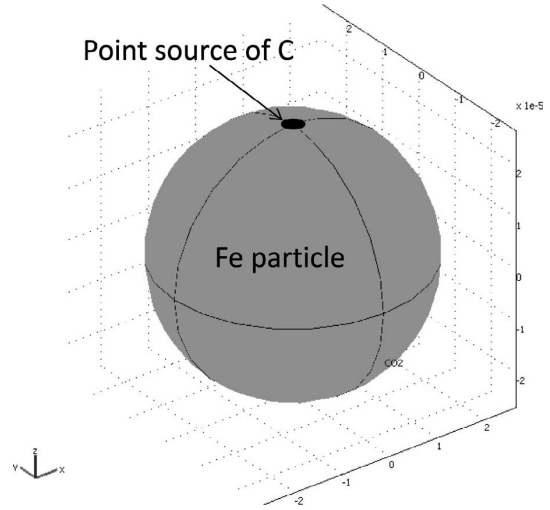

Fig. 11. Schematic diagram of calculation arrangement of a spot source diffusion process.

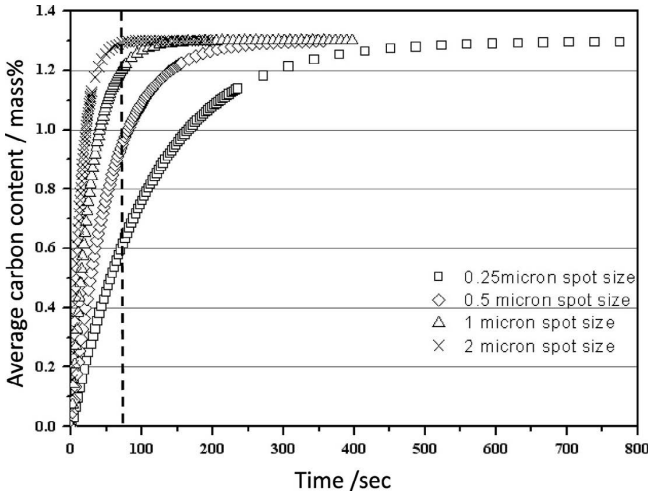

Fig. 12. Average carbon concentrations as a function of time with various spot areas.

that of surface source diffusion. With the spot area's diameter of 2 μm, the average C concentration of the Fe sphere reached to about 1.3 mass% after 60 second. In the actual case, however, the required time is expected to be much more short by the following reasons; (1) the number of contacting spots will be more than one, (2) D_C will increase with the C concentration, (3) the liquid phase formation possibly enhance the C diffusion rate and (4) the diffusion process was not isothermal process but temperature was raising. Actually temperature increased about 25 K between start and finish of metal-slag separation. Taking into account these C diffusion rate enhancing effects, it is reasonable to assume that the C concentration in the iron sphere can reach to the solidus line concentration (1.3 mass C %) within 20–30 second after contacting with carbon.

As shown in Fig. 4, metal-slag separation was finished within about 20 seconds after eutectic slag melting. If most of iron particles existed as liquid phase at around the eutectic slag melting temperature, the pellet will be simultaneously melted down with slag melting. The maintaining the shape of pellets even after eutectic slag melting means that most of iron particles will be existed as solid particles at the

slag melting temperature, or iron was not carburized well before eutectic slag melting. In other words, all iron particles must be melted within 20 seconds after eutectic slag melting. As already discussed, the C concentration in the most iron particle was increased to the solidus line concentration within about 20–30 seconds at 1 573 K. Thus, it is possibly assumed that iron particles melting can be achieved after the slag melting. The metal-slag separation behavior of Cr_2O_3 added $CaO–Al_2O_3$ based slags shown in Fig. 6 can be explained similarly based on the rapid carburization process introduced by the eutectic slag melting.

In the cases of NiO contained $CaO–Al_2O_3$ based slags, the metal-slag separation did not start after the eutectic slag melting but started after the total liquid fraction reached at about 80% as shown in Fig. 8. It is well known that the viscosity of partially molten materials or solid suspension liquid is very large. There are several models to describe the viscosity of these melts, and Roscoe model has been widely used.[16] The relative viscosity of a suspension of rigid solid particles is given by

$$\eta_{\text{eff}} = \eta_{\text{liq}}(1-1.35\Phi)^{-2.5} \quad \text{..... (3)}$$

where, η_{liq} = the liquid viscosity without solid particles (Pa·s), η_{eff} = the effective viscosity (Pa·s), Φ = the volume percentage of all the solid phases. The density diffrence between solid and liquid slag is small so that the volume fraction can be assume to close to the mass fraction. Generally molten slags with large solid phase fraction have high viscosity. For example, the slag visicosity with Φ = 0.7 became 1 400 times larger than that without solid phase. Even with Φ = 0.5, it has 16 times larger value. The high viscosity slags could prevent the spread out of slag on the solid iron surface. Consequently, iron carburization was delayed. These calculations suggested that the existence of large amount of slag without solid particles suspension will be preferable for easy metal-slag separation. In other words, the slag composition as close as to the eutectic point is favored for the easy metal- slag separtion.

For the $CaO–Al_2O_3–SiO_2$ based slag (Fig. 10), the metal-slag separation took about 40 seconds after slag melting. It was about 2 times longer than those of $CaO–Al_2O_3$ based slag. As like the case of $CaO–Al_2O_3$ based slags, the molten slag could help to contact carbon and iron particles to promote carburization process. As shown in Fig. 9, the eutectic liquid slag formation temperature of slag H was about 60 K lower than those of high $CaO–Al_2O_3$ based slag. Thus, the carbon diffusion process can start at relatively lower temperature. However, the value of D_C was small at the lower temperature condition and larger carbon concentration was required to reach to the solidus line at lower temperature. These factors could make the carbon diffusion process much slower than those in $CaO–Al_2O_3$ based slag. Namely, the metal-slag separation behavior of slag H can be also explained based on the rapid carburization process introduced by slag melting.

4.3. The Role of Molten Slag

As discussed in the previous section, iron particles were supposed to be rapidly carburized after slag melting. During the carburization process, the contact between iron and graphite particles must be continuously maintained. The contact point, however, will be soon lost after some amount carbon diffused to an iron particle without any pushing forces. Recently Kim *et al.*[8] and Jeong *et al.*[17] investigated 3 phases co-existed interfacial phenomena among slag, iron and carbon particles. Kim *et al.*[8] confirmed that molten slag could introduce the attractive force between iron and graphite particles. After slag melting at a particular temperature, it spread out over the solid Fe and carbon particle surface due to the good wettability of slag on solid iron and carbon. Along with slag spreading, the carbon particle was pulled towards solid iron particle and finally contacted with the iron particles. They found once carbon and Fe particles contacted, these never separated. With developing carburization process with time after the contact, some amount of liquid iron will be formed between carbon and solid Fe particles. Generally liquid iron did not wet with carbon. Jeong *et al.*,[17] however, found out that liquid iron became wet with carbon surface if molten slag was coexisted. Therefore, the produced liquid iron contacted with molten slag and carbon could wet well with the carbon surface so that the contacting area between carbon and liquid Fe particles increased with time and enhanced the apparent carburization rate. These processes are schematically illustrated in **Fig. 13**. Namely, (a) each solid iron and graphite particle came to close after slag melting, and finally (b) they contacted each other. Then (c) the liquid iron phase was formed due to carburization reaction. (d) The contacting area between a graphite particle and liquid iron increased with time since liquid iron wetted well with graphite under molten slag co-existence.

It was already reported that the slag melting behaviour has strong effect on the direct contact carburization reaction by several researchers.[9,18–22] In these studies, the slag melting behaviour means minerals in iron ore and ash in cokes change from solid phase to liquid phase. Matsui *et al.*[19] reported the effect of minerals of iron ore on carburization behaviour. Heru *et al.*[20] and Chapman *et al.*[21] investigated the effect of ash on carburization behaviour. These studies confirmed that easy melting of mineral and ash had an advantage for the carburization reaction. The effect of molten slag in these previous results can be explained by the promotion of the direct contact between carbon and iron particles introduced by slag melting.

4.4. Industrial Applications

All results in the present study and previous studies showed that slag melting had a very important role to achieve clear and easy metal-slag separation. Molten slag provided good contact between iron and graphite particles and also enhanced the carburization rate by assisting the extension of contact area between liquid iron and graphite surface. $CaO–Al_2O_3$ based slag near the eutectic composition produced the large amount of eutectic liquid phase at around 1 573 K, as already mentioned, this melting behavior is preferable for easy metal-slag separation. Along with the good the metal-slag separation, high desulfurization and dephosphorization abilities are expected from $CaO–Al_2O_3$ based slags due to their high basicity. Thus, $CaO–Al_2O_3$ based slags is very effective to use high Al_2O_3 iron ore in CCA reduction process.

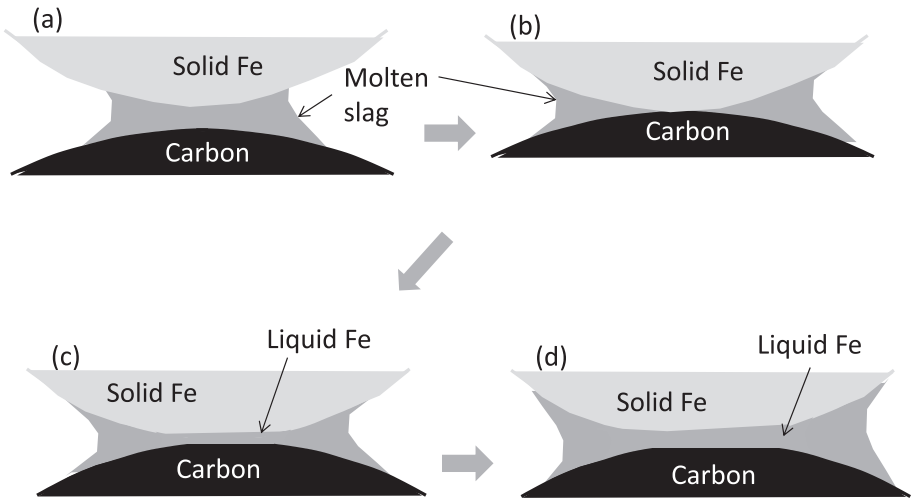

Fig. 13. Schematic views of the carbon and iron particle contact area change with time.

5. Conclusions

The *in-situ* confocal laser-scanning microscope observation of metal-slag separation behaviors between $CaO–Al_2O_3$ based slag, iron and graphite powder mixed pellets were carried out to investigate the feasibility to use high Al_2O_3 iron ore in CCA reduction processes. The observed metal-slag separation behaviors were analyzed based on the equilibrium phase fractions calculated by FactSage and the rate of carbon diffusion in iron particles. The obtained results are summarized as follow:

(1) In $CaO–Al_2O_3$ based slag and that with Cr_2O_3 added slags, the metal-slag separation was found to start after the eutectic slag melt was formed.

(2) In NiO added $CaO–Al_2O_3$ based slags, the metal-slag separation did not start after the eutectic melt formation, but started at the first inflection point after eutectic in liquid fraction curve. High viscosity of liquid with solid particles suspension at around the eutectic melt formation temperature could prevent the spread out of slag on the solid iron surface, and delayed the carburization process.

(3) The carburization of iron particles dominantly occurred after slag melting since molten slag made it possible to maintain the contact between iron and graphite particles.

(4) The carburization rates could be enhanced after liquid iron was formed due to the contact area increase by the good wettability of liquid iron with graphite surface under the molten slag co-existence condition.

(5) The use of $CaO–Al_2O_3$ based slags on CCA reduction process is feasible to meet the demand of low grade high Al_2O_3 iron ore utilization.

REFERENCES

1) L. Lu, R. J. Holmes and J. R. Manuel: *ISIJ Int.*, **47** (2007), 349.
2) A. Cores, A. Babich, M. Muñiz, S. Ferreira and J. Mochon: *ISIJ Int.*, **50** (2010), 1089.
3) H. Michishita and H. Tanaka: *Kobelco Tech. Rev.*, **29** (2010), 69.
4) T. Harada and H. Tanaka: *ISIJ Int.*, **51** (2010), 1301.
5) I. F. Kurunov: *Metallurgist*, **54** (2010), 355.
6) K. Ohno, M. Kaimoto, T. Maeda, K. Nishioka and M. Shimizu: *ISIJ Int.*, **51** (2011), 1279.
7) A. E. A. Nogueira, M. B. Mourao, C. Takano and D. M. dos Santos: *Mater. Res.*, **13** (2010), 191.
8) H. S. Kim, J. G. Kim and Y. Sasaki: *ISIJ Int.*, **50** (2010), 1099.
9) K. Ohno, T. Miki, Y. Sasaki and M. Hino: *ISIJ Int.*, **48** (2008), 1368.
10) K. Saito, K. Ohno, T. Miki, Y. Sasaki and M. Hino: *ISIJ Int.*, **46** (2006), 1783.
11) Verein Deutscher Eisenhüttenleute: Slag Atlas, 2nd Ed., Verlag Stahleisen mbH, Düsseldorf, (1995), 364.
12) H. S. Kim, Y. B. Kang, J. G. Kim and Y. Sasaki: *ISIJ Int.*, **51** (2011), 166.
13) S. Takagi and T. Furui: *Int. J. Miner. Process.*, **19** (1987), 145.
14) M. Hino, T. Nagasaka, A. Katsumata, K. Higuchi, K. Yamaguchi and N. Kon-no: *Metall. Trans. B*, **30B** (1999), 672.
15) J. Ågren: *Scr. Metall.*, **20** (1986), 1507.
16) R. Roscoe: *J. Appl. Phys.*, **3** (1952), 267.
17) I. H. Jeong, H. S. Kim and Y. Sasaki: *ISIJ Int.*, **53** (2013), 2090.
18) S. Kondo and K. Ishii: *Tetsu-to-Hagané*, **70** (1984), A1.
19) T. Matsui, N. Ishiwata, Y. Hara and K. Takeda: *ISIJ Int.*, **44** (2004), 2105.
20) W. Heru, K. Ohno, T. Nagasaka and M. Hino: *CAMP-ISIJ*, **15** (2002), 98.
21) M. W. Chapman, B. J. Monaghan, S. A. Nightingale, J. G. Mathieson and R. J. Nightingale: *ISIJ Int.*, **47** (2007), 973.
22) K. Ohno, T. Miki and M. Hino: *ISIJ Int.*, **44** (2004), 2033.